THE JOURNAL OF PHYSICAL CHEMISTRY C
A JOURNAL OF THE AMERICAN CHEMICAL SOCIETY

pubs.acs.org/JPCC
Article

Theoretical Procedure for Precise Evaluation of Chemical Enhancement in Molecular Surface-Enhanced Raman Scattering

Published as part of The Journal of Physical Chemistry C special issue "Celebrating 50 Years of Surface Enhanced Spectroscopy".

Roberto A. Boto,* Rubén Esteban,* Bruno Candelas, and Javier Aizpurua*

Cite This: J. Phys. Chem. C 2024, 128, 18293−18304

Read Online

ACCESS | Metrics & More | Article Recommendations | Supporting Information

ABSTRACT: The enhancement of the molecular Raman signal in plasmon-assisted surface-enhanced Raman scattering (SERS) results from electromagnetic and chemical mechanisms, the latter determined to a large extent by the chemical interaction between the molecules and the hosting plasmonic nanoparticles. A precise quantification of the chemical mechanism in SERS based on quantum chemistry calculations is often challenging due to the interplay between the chemical and electromagnetic effects. Based on an atomistic description of the SERS signal, which includes the effect of strong field inhomogeneities, we introduce a comprehensive approach to evaluate the chemical enhancement in SERS, which conveniently removes the electromagnetic contribution inherent to any quantum calculation of the Raman polarization. Our approach uses density functional theory (DFT) and time-dependent DFT to compute the total SERS signal, together with the electromagnetic and chemical enhancement factors. We apply this framework to study the chemical enhancement of biphenyl-4,4′-dithiol embedded between two gold clusters. Although we find that for small clusters the total SERS enhancement is mainly determined by the chemical mechanism, our procedure enables removal of the electromagnetic contribution and isolation of the contribution of the bare chemical effect. This approach can be applied to reproduce and understand Raman line activation and strength in practical and challenging SERS configurations such as in plasmonic nano- and pico-cavities.

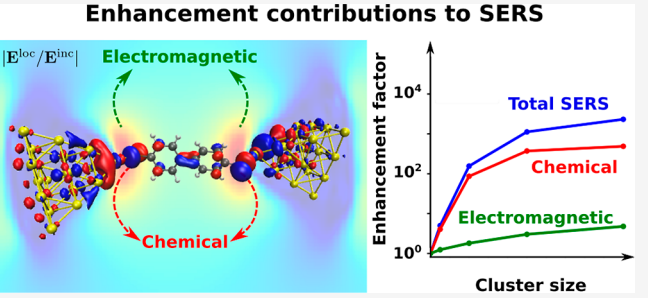

1. INTRODUCTION

Surface-enhanced Raman scattering (SERS) is a molecular spectroscopy technique based on the enhancement of the Raman signal of molecules located near metallic surfaces, thanks to the excitation of localized surface plasmons.[1,2] First discovered by Fleishman et al.[3] in 1974, SERS is today a mature technique for molecular detection and quantitative characterization with applications in strategic fields such as biosensing,[4−6] electrochemistry,[7] food industry,[8,9] and photovoltaics cells,[10,11] to cite a few.

The enhancement factor of the molecular Raman signals in SERS is often estimated to range[12] from ∼10^5 to ∼10^{11} and has been traditionally ascribed to two independent mechanisms: the electromagnetic (EM) and the chemical (CHEM) mechanisms. The EM mechanism results from the enhanced and strongly confined EM field sustained by the localized surface plasmons, and it is usually considered to be the main contribution to the SERS enhancement factor.[13−23] Under certain conditions,[24,25] the contribution of the EM mechanism to the SERS enhancement factor can be as large as 10^{10}. In contrast, the CHEM mechanism in (electronically) nonresonant SERS arises from the chemical interaction between the molecules and the metallic surface of the plasmonic active nanostructure.[26−31] Quantum chemistry calculations within density functional theory (DFT) of molecules interacting with plasmonic surfaces predict that the CHEM mechanism can contribute with a factor of up to 10^3 to the nonresonant SERS enhancement.[32−34]

The interplay between the EM and CHEM mechanisms is not yet fully and systematically captured. Common approaches to evaluate the contribution from both mechanisms to the total SERS enhancement assume that both contributions can be obtained independently using different approaches.[32,33,35,36] The EM contribution is calculated from the plasmonic response of the hosting metallic nanostructure, as obtained by solving the classical Maxwell's equations. The contribution of the CHEM mechanism is computed by solving the

Received: May 27, 2024
Revised: August 20, 2024
Accepted: August 22, 2024
Published: October 17, 2024

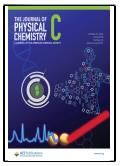

Schrödinger equation (typically using DFT) of a model system consisting of a molecule interacting with small metallic clusters that mimic the environment of the molecule in SERS experiments. This later approach typically assumes that the enhancement obtained from the DFT calculations is only due to the CHEM mechanism and often approximates the Raman polarizability with a two-state model.[33,37,38] However, the solution of the Schrödinger equation also captures, in principle, all the polarization-driven enhancing effects in the system, including the local enhancement of the EM fields produced by the polarization of the metallic clusters, which underlies the EM mechanism. By assuming that only the CHEM mechanism is responsible for the enhancement in such small metallic clusters, its magnitude could be overestimated. Attempts to isolate the contribution of the EM mechanism to the SERS enhancement factor have also been implemented in previous studies by solving the Schrödinger equation using semi-empirical methods.[38,39]

In this work, we present a comprehensive approach based on full ab initio calculations to quantitatively extract the CHEM contribution from the total SERS enhancement factor by subtracting the EM contribution and apply this methodology to a canonical system of an organic molecule in a metallic gap formed by two clusters. This approach uses DFT calculations to obtain the Raman polarizability of the molecule attached to the small metallic clusters, time-dependent DFT (TDDFT) simulations to obtain the EM fields induced by the metallic clusters, and the calculation framework developed by Zhang et al. to address Raman spectroscopy under inhomogeneous EM fields.[40,41] By applying this methodology, we are able to quantify the CHEM contribution to the SERS signal emitted by the molecule biphenyl-4,4′-dithiol (BPDT), embedded in two gold clusters formed by up to 1, 4, 10, and 20 atoms each that represent the chemical environment of the molecule when it lies in a plasmonic cavity.

2. THEORETICAL METHODS

We optimize all the structures with the code Gaussian16[42] using DFT. To obtain the structure of the gold clusters, we first optimize the structure of the gold cluster formed by 20 atoms with the exchange−correlation functional B3P86,[43,44] as this functional yields structures with harmonic frequencies that agree well with experimental values,[45] and the basis set LANL2DZ.[46] We use this structure to obtain the structures of the clusters of 10 and 4 gold atoms by removing 10 and 16 atoms, respectively. We then build the gaps formed by two clusters in the tip-to-tip configuration. To optimize the BPDT molecule in the complex $[Au_n\text{-BPDT-}Au_n]^{2+}$ (n = 4, 10, 20), we follow a two-step procedure: we first optimize the separation distance between the clusters (gap thickness); we then relax the structure of the molecule inside the gap using the optimized separation distances obtained in the first step (see Section S7 in the Supporting Information for further details).

In the first of these two steps, we optimize the gap thickness. We selected an initial separation distance of 19 Å between the gold clusters and placed the molecule inside the gap. The interaction between the molecule and the clusters impacts their configuration (symmetry and orientation), thus modifying the configuration of the gap. To account for the effect of the interaction between the molecule and the gold atoms on the gap thickness but without altering the configuration of the gap, we replace the hydrogen atoms attached to the sulfur atoms with gold atoms. We then relax the structure of the BPDT molecule with the single gold atoms attached but freeze the position of the atoms of the clusters, so their positions are not altered during the optimization process. We use in this step the standard B3LYP exchange−correlation functional[43] and the basis set 6-31G(d,p)[47] for the carbon, hydrogen, and sulfur atoms. For the gold atoms, we use the LANL2DZ basis set.[46] We define the gap thickness as the distance between the gold atoms attached to the sulfur atoms, and thus the optimized separation distances are 13, 14, and 14 Å for the gaps formed by the clusters of 20, 10, and 4 gold atoms, respectively. In the case of the gap formed by two gold atoms in $[Au\text{-BPDT-}Au]^{2+}$, we select a separation distance of 15 Å as we observed that for shorter distances, the two gold atoms reduce the symmetry of the molecule.

In the second step, we use the separation distances obtained previously to optimize the structure of the molecule in the complex $[Au_n\text{-BPDT-}Au_n]^{2+}$ (n = 1, 4, 10, and 20). In this step, we remove the single gold atom placed between the molecule and the clusters, so that the molecule is directly bonded to the clusters. We use the standard B3LYP, exchange−correlation functional,[43] which produces fundamental frequencies in good agreement with experimental measurements,[45] and the basis set 6-31G(d,p) for the carbon, hydrogen, and sulfur atoms. For the gold atoms in the complex $[Au_n\text{-BPDT-}Au_n]^{2+}$ (n = 1, 4, 10, and 20), we use the LANL2DZ basis set.[46] To account for noncovalent interactions, we add the empirical dispersion correction D3 of Grimme et al.[48] with the damping function of Becke and Johnson (BJ).[49] During optimization of the molecular structure, we freeze the positions of the gold atoms. Thus, we avoid that atomic displacements of the gold atoms in the clusters could modify the configuration (distance and orientation) of the cluster dimers (see Section S11 in the Supporting Information for calculations of relaxed cluster structures). Similarly, we freeze the positions of the gold atoms during the calculation of the vibrational modes to remove the effect of modes delocalized between the clusters and the molecule. To ensure that the frontier molecular orbitals are localized in the molecule, we compute all of the complexes $[Au_n\text{-BPDT-}Au_n]$ with charge +2 atomic units (a.u.). Vibrational frequency analysis does not reveal any imaginary frequency confirming that all the molecular structures correspond to the minima of the potential energy surface. We use the same theory level to compute the vibrational frequencies, as well as the Raman polarizabilities in the absence ($\vec{\vec{\alpha}}^{\mathrm{Ram}}$) and in the presence ($\vec{\vec{\alpha}}^{\mathrm{SERS}}$) of the gold clusters.

To obtain the induced Raman dipole of the molecule in free-space $\boldsymbol{p}^{\mathrm{Ram}}$, we compute $\vec{\vec{\alpha}}^{\mathrm{Ram}}$ for the molecule oriented in such a way that the main molecular axis (the axis defined by the line that connects the sulfur atoms) is parallel to the z-direction. We then compute $\boldsymbol{p}^{\mathrm{Ram}}$ from $\vec{\vec{\alpha}}^{\mathrm{Ram}}$ for incident light polarized along the z-direction of energy 0.5 eV and a temperature of 289.15 K. For the calculations of the Raman signal scattered by the molecule bonded to the gold clusters, we rotate the clusters such that the gap between them is aligned along the z-direction and compute the induced Raman dipole $\boldsymbol{p}^{\mathrm{SERS}}$ using the Raman polarizability of the Au_n-BPDT-Au_n complex, $\vec{\vec{\alpha}}^{\mathrm{SERS}}$ and considering again incident light polarized along the z-direction of energy 0.5 eV. The energy of the incident light is away from any electronic resonance of the molecule and from EM resonances of the cluster and thus facilitates the extraction of the (nonresonant) chemical enhancement.

https://doi.org/10.1021/acs.jpcc.4c03491
J. Phys. Chem. C 2024, 128, 18293−18304

To obtain the EM contribution to the SERS enhancement, we compute the local EM field E^{loc} for each cluster dimer in vacuum. First, we compute the ground state of the cluster dimers with the SIESTA package,[50] using the PBE functional,[51,52] which has also been shown to correctly reproduce the optical response of small cluster nanoparticles,[53] and a double-ζ polarized basis set as implemented therein. We then compute the EM fields induced by an incident plane-wave polarized along the z-axis direction on a regular grid using the efficient linear-response method implemented in the PyNAO (Python Numeric Atomic Orbitals) code,[54] and the same exchange−correlation functional and basis set used to obtain the ground state of the cluster dimers. To obtain the induced Raman dipole of the molecule within the EM field induced by the clusters ($\boldsymbol{p}^{\mathrm{EM}}$) in eq 3, we evaluated the local EM field at the atomic positions corresponding to the molecular structures obtained with DFT by interpolating the previously computed induced fields on the regular grid.

Molecule−cluster aggregates often exhibit charge-transfer excitations whose accurate description requires range-separated corrected DFT functionals. We study in Section S9 of the Supporting Information the impact of charge-transfer effects on the Raman signal by comparing the Raman spectra obtained with B3LYP-D3(BJ) and CAM-B3LYP-D3(BJ),[55] the latter properly accounting for charge-transfer excitations. We show that for off-resonance conditions and for the selected systems, the Raman spectra computed with these two functionals do not affect the conclusions significantly.

3. RESULTS AND DISCUSSION

3.1. Raman Spectrum of BPDT. We first address the Raman signal of the molecule of choice, bare BPDT molecule (molecular structure shown in the inset of Figure 1a). We plot in Figure 1a the Raman spectrum of BPDT in free-space between 200 cm^{-1} and 1800 cm^{-1}, where we display the Stokes differential Raman cross-sections $\left(\frac{\mathrm{d}\sigma_k^{\mathrm{Ram}}}{\mathrm{d}\Omega}\right)$ computed in the 90°-scattering configuration, corresponding to detecting the light[56] emitted in a direction perpendicular to the direction and polarization of the incoming light as a function of the wavenumber of the vibrational excitations (ν_k). For the bare BPDT molecule, we compute $\frac{\mathrm{d}\sigma_k^{\mathrm{Ram}}}{\mathrm{d}\Omega}$ for an oscillating dipole in free-space as

$$\frac{\mathrm{d}\sigma_k^{\mathrm{Ram}}}{\mathrm{d}\Omega} = \frac{(\omega_{\mathrm{inc}} - \omega_k^{\mathrm{Ram}})^4}{16\pi^2 c_0^4 \varepsilon_0^2 |E^{\mathrm{inc}}|^2} \frac{|\boldsymbol{e}^{\mathrm{rad}} \cdot \boldsymbol{p}^{\mathrm{Ram}}|^2}{(1 - \mathrm{e}^{-\hbar\omega_k^{\mathrm{Ram}}/(k_{\mathrm{B}}T)})}$$
$$= \frac{(\omega_{\mathrm{inc}} - \omega_k^{\mathrm{Ram}})^4}{16\pi^2 c_0^4 \varepsilon_0^2 |E^{\mathrm{inc}}|^2} \frac{|\sum_{i,j=1}^{3} e_i^{\mathrm{rad}} \alpha_{ij}^{\mathrm{Ram}} E_j^{\mathrm{inc}}(\omega_{\mathrm{inc}})|^2}{(1 - \mathrm{e}^{-\hbar\omega_k^{\mathrm{Ram}}/(k_{\mathrm{B}}T)})} \quad (1)$$

with ε_0 the vacuum permittivity, c_0 the speed of light in free-space, k_{B} the Boltzmann constant, T the temperature, and ω_{inc} the angular frequency of the incident EM field E^{inc}. ω_k^{Ram}, p^{Ram}, and $\alpha_{ij}^{\mathrm{Ram}}$ are the angular frequencies of the Stokes signal, the induced Raman dipole moment, and the element i-th, j-th of the Raman polarizability tensor $\ddot{\boldsymbol{\alpha}}^{\mathrm{Ram}}$ of the vibrational mode ν_k. $E_j^{\mathrm{inc}}(\omega_{\mathrm{inc}})$ is the j-th component of the amplitude of the incoming EM field E^{inc} at frequency ω_{inc}, and $\boldsymbol{e}^{\mathrm{rad}}$ a unit vector along the direction of the polarization of the emitted EM field. To obtain $\boldsymbol{p}^{\mathrm{Ram}}$, we calculate $\ddot{\boldsymbol{\alpha}}^{\mathrm{Ram}}$ and ω_k^{Ram} using DFT with the exchange−correlation functional B3LYP-D3(BJ)[43,48,49] and the basis set 631-G(d,p).[47] In the following, we consider nonresonant Raman scattering, and therefore, we use incident light of energy $\hbar\omega_{\mathrm{inc}}$ = 0.5 eV ($\hbar$ is the reduced Planck's constant; $\omega_{\mathrm{inc}}/2\pi$ = 120.9 THz or ω_{inc} = 759.6 × 10^{12} rad s^{-1}), significantly lower than any electronic resonances of the molecule. The incident and the emitted light are polarized along the z-axis.

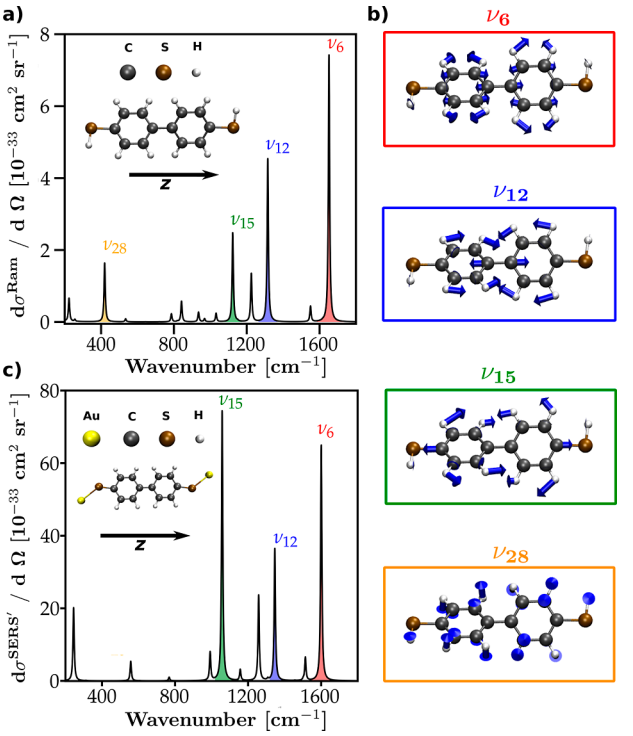

Figure 1. Raman spectrum of biphenyl-4,4′-dithiol (BPDT): (a) Stokes differential Raman cross-section ($\mathrm{d}\sigma^{\mathrm{Ram}}/\mathrm{d}\Omega$) of the bare BPDT molecule as a function of the vibrational wavenumber between 200 cm^{-1} and 1800 cm^{-1}. The inset shows a molecular model of the minimum energy structure of BPDT, where the gray, white, and brown spheres represent the atoms of carbon, hydrogen, and sulfur, respectively. (b) Atomic displacements (blue arrows) corresponding to the vibrational modes ν_6 (red rectangle), ν_{12} (blue rectangle), ν_{15} (green rectangle), and ν_{28} (orange rectangle) of BPDT. The wavenumber of these modes are 1652 cm^{-1}, 1315 cm^{-1}, 1123 cm^{-1}, and 420 cm^{-1}, for ν_6, ν_{12}, ν_{15}, and ν_{28}, respectively. (c) Stokes differential Raman cross-section ($\mathrm{d}\sigma^{\mathrm{SERS}'}/\mathrm{d}\Omega$) as a function of the wavenumber between 200 cm^{-1} and 1800 cm^{-1} for $[\mathrm{Au\text{-}BPDT\text{-}Au}]^{2+}$, where we replace the hydrogen atoms bonded to the sulfur atoms with gold atoms. The inset shows a molecular model of the minimum energy structure of $[\mathrm{Au\text{-}BPDT\text{-}Au}]^{2+}$, where the gray, white, brown, and yellow spheres represent the atoms of carbon, hydrogen, sulfur, and gold, respectively. $\mathrm{d}\sigma^{\mathrm{Ram}}/\mathrm{d}\Omega$ (a) and $\mathrm{d}\sigma^{\mathrm{SERS}'}/\mathrm{d}\Omega$ (c) are computed at 298.15 K and with an incident light of energy 0.5 eV polarized along the z-axis. The spectral lines are broadened by a Lorentzian function of width 8 cm^{-1}. The Raman lines of the vibrational modes ν_6, ν_{12}, ν_{15} and ν_{28} are colored in red, blue, green and orange, respectively.

As shown in Figure 1a, within the 200−1800 cm^{-1} range, the most intense vibrational modes of BPDT are at wavenumbers 1652 cm^{-1}, 1315 cm^{-1}, 1123 cm^{-1}, and 420 cm^{-1} that we label as ν_6, ν_{12}, ν_{15}, and ν_{28}, respectively (labeled following Mulliken's prescriptions[57]). The vibrational modes ν_6 and ν_{12} correspond to combinations of C−H bending and C−C stretching modes of the phenyl rings (see Figure 1b). The

https://doi.org/10.1021/acs.jpcc.4c03491
J. Phys. Chem. C 2024, 128, 18293−18304

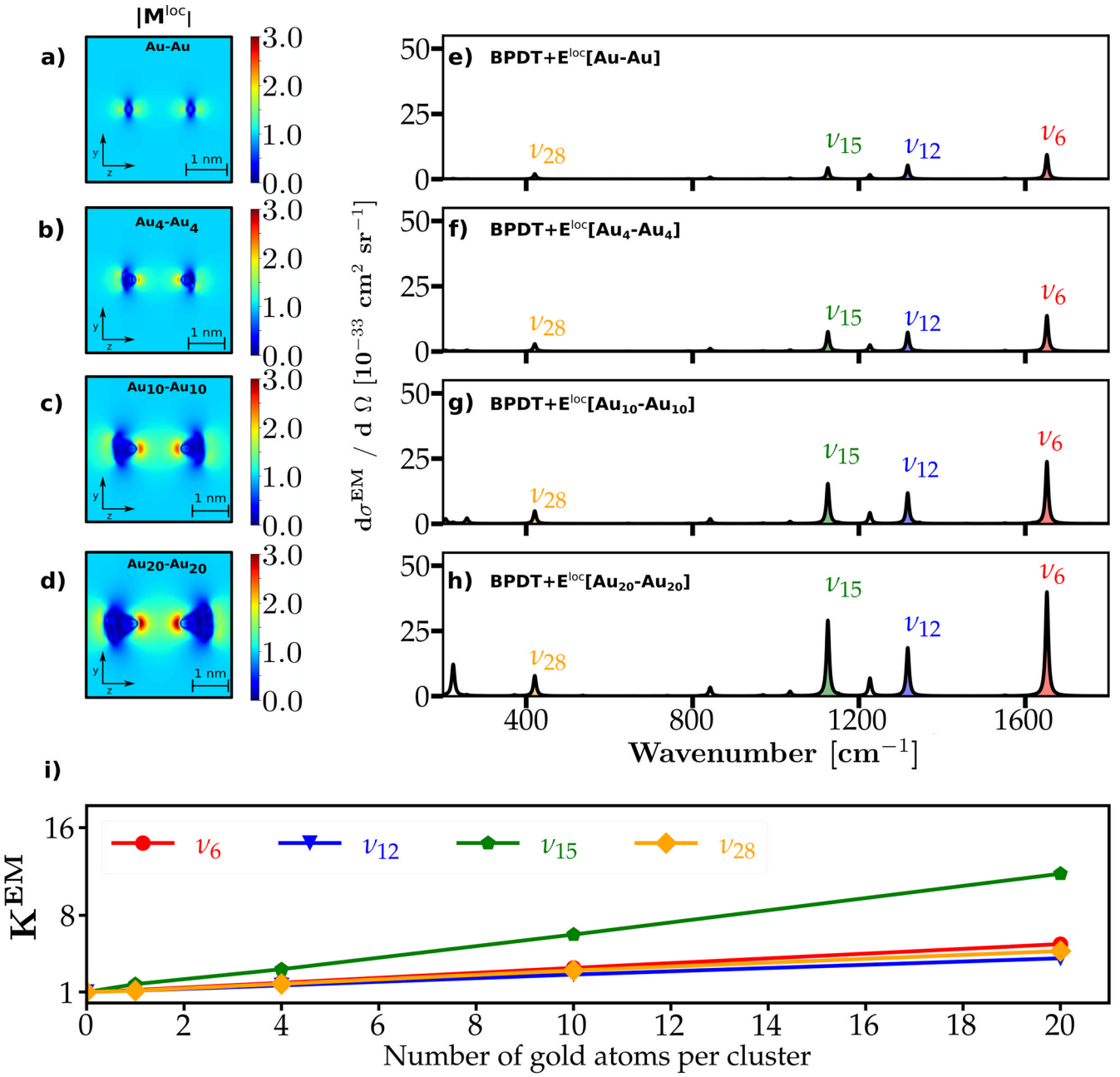

Figure 2. Effect of the EM field on the Raman spectra of BPDT: (a–c) map of the spatial distribution of the field enhancement amplitude ($|M^{loc}|$) near the gold dimers Au–Au (a), Au_4–Au_4 (b), Au_{10}–Au_{10} (c), and Au_{20}–Au_{20} (d). $|M^{loc}|$ is plotted under illumination by a plane wave of energy 0.5 eV polarized along the z-direction of the dimer axis. The local field is calculated in the absence of the molecule. (e–h) Stokes differential Raman cross-section including only the EM enhancement ($d\sigma^{EM}/d\Omega$) as a function of the wavenumber between 200 cm^{-1} and 1800 cm^{-1}, for BPDT in the local field induced by the dimers of the clusters. We consider that the number of atoms in each of the two gold clusters is one (BPDT + E^{loc}[Au–Au], (e)), four (BPDT + E^{loc}[Au_4–Au_4], (f)), ten (BPDT + E^{loc}[Au_{10}–Au_{10}], (g)), and twenty (BPDT + E^{loc}[Au_{20}–Au_{20}], (h)). $d\sigma^{EM}/d\Omega$ is obtained at 298.15 K and with an incident light of energy 0.5 eV polarized along the z-axis. The spectral lines are broadened by a Lorentzian function of width 8 cm^{-1}. The Raman lines of the vibrational modes ν_6, ν_{12}, ν_{15}, and ν_{28} are colored in red, blue, green, and orange, respectively. (i) Evolution of the EM enhancement factor (K^{EM}, from eq 5) with increasing size of the gold clusters for each of the vibrational modes ν_6 (solid red line), ν_{12} (solid blue line), ν_{15} (solid green line), and ν_{28} (solid orange line).

vibrational mode ν_{15} is characterized by stretching of the C–S bonds, and the vibrational mode ν_{28} corresponds to out-of-plane bendings of the phenyl rings.

When the molecule is sandwiched between two gold surfaces, the intensity of the Raman lines undergoes an enhancement due to the EM field induced by the gold surfaces (EM mechanism) and the chemical interaction between the molecule and the surfaces (CHEM mechanism).[40] To illustrate the (predominantly) chemical enhancement that is already present for a very small number of gold atoms, we show in Figure 1c the Raman spectrum of BPDT where the sulfur atoms are bound to one gold atom each $[Au\text{-}BPDT\text{-}Au]^{2+}$ (molecular structure shown in the inset of Figure 1c), instead of to hydrogen atoms as in the bare molecule case. To compute the Stokes differential Raman cross-section for $[Au\text{-}BPDT\text{-}Au]^{2+}$, we first optimize the molecular structure within

https://doi.org/10.1021/acs.jpcc.4c03491
J. Phys. Chem. C 2024, 128, 18293–18304

DFT using the exchange−correlation functional B3LYP-D3(BJ)[43,48,49] and the basis set 6-31G(d,p)[47] for the atoms of hydrogen, carbon, and sulfur, and the basis set LANL2DZ[46] for the atoms of gold (see Theoretical Methods for further details on the quantum chemistry calculations). During optimization, we freeze the position of the gold atoms. Then, we perform the vibrational analysis of the optimized structure using the same DFT exchange−correlation functional and basis sets as for the optimization of the molecular structure. To isolate the native vibrations of the molecule from those delocalized between the molecule and the gold atoms, we also freeze the positions of the gold atoms during the vibrational analysis. We illustrate the effect of the vibrations of the gold atoms on the molecular Raman signal in Figure S3 of the Supporting Information.

In this initial calculation, we obtain the Stokes differential Raman cross-section $\left(\frac{d\sigma_k^{SERS'}}{d\Omega}\right)$ for a 90°-scattering configuration by following the approach typically used in the literature, which considers that the induced Raman dipole of the molecule ($\boldsymbol{p}^{SERS}$) emits in free-space.[32,39,58−62] In this case

$$\frac{d\sigma_k^{SERS'}}{d\Omega} = \frac{(\omega_{inc} - \omega_k^{SERS})^4}{16\pi^2 c_0^4 \varepsilon_0^2 |E^{inc}|^2} \frac{|\boldsymbol{e}^{rad}\cdot\boldsymbol{p}^{SERS}|^2}{(1 - e^{-\hbar\omega_k^{SERS}/(k_B T)})} = \frac{(\omega_{inc} - \omega_k^{SERS})^4}{16\pi^2 c_0^4 \varepsilon_0^2 |E^{inc}|^2} \frac{|\sum_{i,j=1}^{3} e_i^{rad}\alpha_{ij}^{SERS} E_j^{inc}(\omega_{inc})|^2}{(1 - e^{-\hbar\omega_k^{SERS}/(k_B T)})} \quad (2)$$

with ω_k^{SERS} the Stokes angular frequency and α_{ij}^{SERS} the i-th and j-th element of the induced Raman dipole tensor $\vec{\vec{\alpha}}^{SERS}$ of the vibrational mode ν_k of the BPDT molecule bound to the gold atoms, as obtained from DFT calculations. By comparing Figure 1a with Figure 1c, we can observe that the presence of the gold atoms induces substantial changes in the Raman spectrum of BPDT. For instance, the vibrational mode ν_{28} becomes almost dark due to the drastic reduction of the dihedral angle between the phenyl rings that turns the molecule flat and therefore changes the molecular symmetry (the Raman line of the vibrational mode ν_{28} cannot be appreciated in Figure 1c because it appears out of scale). Moreover, the strengths of the Raman lines of the vibrational modes ν_6, ν_{12}, and ν_{15} are enhanced by about a factor 10 due to the bonding of the molecule with the gold atoms (inset of Figure 1c). Interestingly, in the low-frequency region, the vibrational mode ν_{42} at 224 cm^{-1} (Au−S stretching mode, not highlighted in Figure 1) is also strongly enhanced by the gold atoms (see Section S10 of the Supporting Information for further discussion on the mode ν_{42}). Usually, this enhancement is directly associated with the CHEM mechanism of SERS enhancement. This assumption is expected to be accurate for the situation considered in Figure 1c, with only one gold atom attached at each end of the molecule. However, including a larger number of gold atoms in the DFT calculation (as necessary for an accurate determination of the SERS chemical enhancement) also strengthens the EM field induced by the gold atoms, introducing an EM contribution to the value of $\boldsymbol{p}^{SERS}$ on top of the pure chemical effect and thus making the quantification of the pure chemical enhancement less straightforward. We further note that eq 2 connects $\boldsymbol{p}^{SERS}$ with the cross section by using the expression of the emission of a dipole under vacuum. However, the EM interaction between the molecule and the gold atoms can further increase the emission (Section S4 of the Supporting Information). Thus, eq 2 contains part but not all of the EM contribution to the enhancement.

In the following section, we discuss how to separate the chemical and EM contributions to the SERS enhancement by quantitatively monitoring each contribution for two tetrahedral gold clusters (formed by up to 1, 4, 10, and 20 atoms each) embedding the molecule.

3.2. Electromagnetic Enhancement. We focus first on quantifying the EM contribution to the enhancement of the molecular Raman signal of the BPDT molecule sandwiched between two Au_n clusters containing 1, 4, 10, and 20 atoms each, that we label as Au_n (n = 1, 4, 10, and 20). The enhancement of the molecular Raman signal due to the EM mechanism is a consequence of the enhancement of the local EM field induced by the gold clusters $E^{loc}(\boldsymbol{r}, \omega) = M^{loc}(\boldsymbol{r}, \omega) E^{inc}(\boldsymbol{r}, \omega)$ with $E^{loc}(\boldsymbol{r}, \omega)$ and $E^{inc}(\boldsymbol{r}, \omega)$ the local and the incident EM field at position $\boldsymbol{r}$ and frequency ω, respectively. This enhancement facilitates the excitation of the induced Raman dipole, $\boldsymbol{p}^{Ram} \propto M^{loc}(\boldsymbol{r}, \omega_{inc})$, and boosts the light emitted by this dipole (as we will see below). Since the clusters are small (the volume of the largest cluster is approximately 0.06 nm^3), using classical calculations to compute $E^{loc}(\boldsymbol{r}, \omega)$ is questionable. Thus, we obtain $E^{loc}(\boldsymbol{r}, \omega)$ and $M^{loc}(\boldsymbol{r}, \omega)$ using linear-response TDDFT with the exchange−correlation functional PBE[51,52] and a double-zeta polarized basis set.[54]

We show in Figure 2a−d the spatial distribution of the local EM field enhancement $|M^{loc}(\boldsymbol{r}, \omega_{inc})|$ near the gold clusters of the four different sizes considered, illuminated by an electromagnetic planewave with electric field polarized along the direction of the gap (z-axis) of energy 0.5 eV. These simulations consider only the metallic clusters (without the molecule), but the position of the Au atoms is the same as in the situation with the molecule $[Au_n\text{-BPDT-}Au_n]^{2+}$. We obtain the selected metallic clusters from the minimum energy structure of the gold cluster formed by 20 atoms and with tetrahedral symmetry optimized within DFT using the exchange−correlation functional B3P86[43,44] and the basis LANL2DZ.[46] To build up the gap, we align the tetrahedral cluster across the gap in the tip-to-tip configuration with the apexes of the clusters pointing to each other and select a separation distance between the clusters of 13 Å, so that the molecule can fit inside the gap. We build up the gap for the clusters of 10 and 4 gold atoms by removing atoms of the gap formed by the Au_{20} clusters without further optimization and selecting a separation distance between the clusters of 14 Å. For the gap formed by two gold atoms, we use a separation distance of 15 Å (see the section on theoretical methods for further details on the selection of the separation distance between the clusters).

As the number of gold atoms, n, increases from 1 to 20, the local EM field becomes localized at a small region in the gap between the two clusters, around the gold atoms at the tip of the tetrahedrons, mostly due to a lighting rod effect.[53] The fields are strongly inhomogeneous spatially, so that, when a molecule is placed in the gap, the different atoms of the molecule experience local fields of very different strengths.[63,64]

To account for the effect of the inhomogeneity of $E^{loc}(\boldsymbol{r}, \omega_{inc})$ on the Stokes differential Raman cross-section,[41] we first compute the induced Raman dipole of the molecule induced by the local field, $\boldsymbol{p}^{EM}$ (the superindex EM emphasizes that we are only considering the effect of the EM enhancement on

https://doi.org/10.1021/acs.jpcc.4c03491
J. Phys. Chem. C 2024, 128, 18293−18304

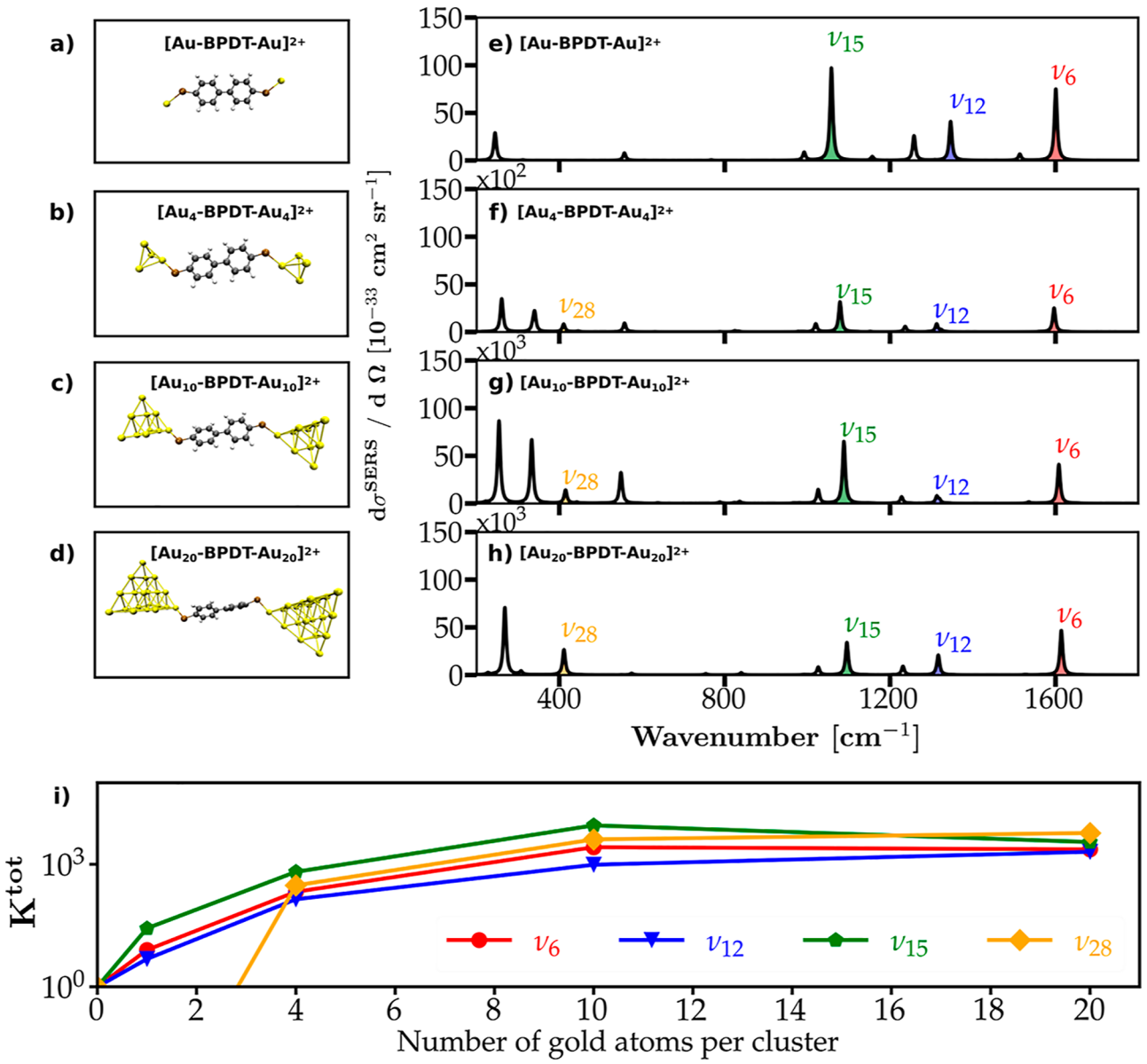

Figure 3. SERS spectra of $[Au_n\text{-BPDT-}Au_n]^{2+}$ (n= 1, 4, 10, and 20): (a−c) Molecular models of the minimum energy structures of the molecule in $[Au\text{-BPDT-}Au]^{2+}$ (a), $[Au_4\text{-BPDT-}Au_4]^{2+}$ (b), $[Au_{10}\text{-BPDT-}Au_{10}]^{2+}$ (c), and $[Au_{20}\text{-BPDT-}Au_{20}]^{2+}$ (d), where the gray, white, brown, and yellow spheres represent the atoms of carbon, hydrogen, sulfur, and gold, respectively. (d−f) Stokes differential Raman cross-section ($d\sigma^{SERS}/d\Omega$) as a function of the wavenumber between 200 cm^{-1} and 1800 cm^{-1} for $[Au\text{-BPDT-}Au]^{2+}$ (e), $[Au_4\text{-BPDT-}Au_4]^{2+}$ (f), $[Au_{10}\text{-BPDT-}Au_{10}]^{2+}$ (g), and $[Au_{20}\text{-BPDT-}Au_{20}]^{2+}$ (h). $d\sigma^{SERS}/d\Omega$ is computed at 298.15 K and with an incident light of energy 0.5 eV and polarized along the axis of the clusters (z-axis). The spectral lines are broadened by a Lorentzian function of width 8 cm^{-1}. The Raman lines of the vibrational modes ν_6, ν_{12}, ν_{15}, and ν_{28} are colored in red, blue, green, and orange, respectively. Notice the different scales of the spectra [scale factors for panels (f−h) on the upper-right corner of the corresponding spectrum]. (i) Evolution of the total SERS enhancement factor (K^{tot}) with the size of the gold clusters for the vibrational modes ν_6 (solid red line), ν_{12}(solid blue line), ν_{15} (solid green line), and ν_{28} (solid orange line). Notice the logarithmic scale used to plot the values of the y-axis

$\boldsymbol{p}^{Ram}$). To obtain $\boldsymbol{p}^{EM}$, we decompose the Raman tensor into atomic contributions.[41] Then, we assume that the induced local dipole at each atom can be obtained by multiplying the atomic Raman tensor by the value of $E^{loc}(\boldsymbol{r}, \omega_{inc})$ at the position of the corresponding atom

$$p_i^{EM} = \sum_{a=1}^{N_{atoms}} p_{a,i}^{EM} = \sum_{a=1}^{N_{atoms}} \sum_{j=1}^{3} \alpha_{a,ij}^{Ram} E_j^{loc}(\boldsymbol{r}_a, \omega_{inc}) \quad (3)$$

with p_i^{EM} the i-th component of p^{EM}, $p_{a,i}^{EM}$ the i-th component of the atomistic induced Raman dipole of the atom a, $\alpha_{a,ij}^{Ram}$ the i-th, j-th element of the atomistic Raman polarizability tensor $\overleftrightarrow{\boldsymbol{\alpha}}_a^{Ram}$ of atom a (see Section S2 of the Supporting Information for further details on the decomposition of the Raman polarizability tensor into contributions from each atom), and $E_j^{loc}(\boldsymbol{r}_a, \omega_{inc})$ the value of the j-th component of the local EM field at frequency ω_{inc} (see Section S2 of the Supporting Information for the complete derivation of eq 3).[41] $E_j^{loc}(\boldsymbol{r}_a,\omega_{inc})$ corresponds to the values of the local field amplitude obtained within TDDFT (in the absence of the molecule but evaluated at the position $\boldsymbol{r}_a$ where the gold atoms a would be located), as represented in Figure 2a−d. $\overleftrightarrow{\boldsymbol{\alpha}}_a^{Ram}$ is obtained without the gold

https://doi.org/10.1021/acs.jpcc.4c03491
J. Phys. Chem. C 2024, 128, 18293−18304

clusters but for the same position and orientation of the molecule as in the complexes $[Au_n\text{-BPDT-}Au_n]^{2+}$. We then remove the contributions of the hydrogen atoms of the thiol groups from the sum in eq 3 as these atoms are absent in the complexes $[Au_n\text{-BPDT-}Au_n]^{2+}$.

To obtain $\frac{d\sigma_k^{EM}}{d\Omega}$ from $\boldsymbol{p}^{EM}$, we invoke the reciprocity theorem,[65] which states that under adequate conditions the electric field amplitude of the light emitted by a dipole (in this case, the induced Raman dipole created at each atom) is proportional to the local field enhancement, in this case at the frequency of emission ω_{rad}, i.e. the emitted intensity is proportional to $|M^{loc}(\omega_{rad})|^2$. Thus, we obtain

$$\frac{d\sigma_k^{EM}}{d\Omega} = \frac{(\omega_{inc} - \omega_k^{Ram})^4}{16\pi^2 c_0^4 \epsilon_0^2 |E^{inc}|^2} \frac{|\sum_{a=1}^{N_{atoms}} \sum_{i=1}^{3} p_{a,i}^{EM} M_i^{loc}(\boldsymbol{r}_a, \omega_{rad})|^2}{(1 - e^{-\hbar\omega_k^{Ram}/(k_B T)})} \quad (4)$$

with $M^{loc}(\boldsymbol{r}_a, \omega)$ the local field enhancement factor at frequency ω at the position of atom a. We define the EM enhancement factor (K^{EM}) for a given vibrational mode as the ratio of the Raman signal of the molecule emitted with (eq 4) and without (eq 1) the gold clusters, which gives

$$K^{EM} = \frac{|\sum_{a=1}^{N_{atoms}} \sum_{i=1}^{3} p_{a,i}^{EM} M_i^{loc}(\boldsymbol{r}_a, \omega_{Rad})|^2}{|\sum_{a=1}^{N_{atoms}} \sum_{i=1}^{3} e_i^{rad} p_{a,i}^{Ram}|^2} = \frac{|\sum_{a=1}^{N_{atoms}} \sum_{i,j=1}^{3} \alpha_{a,ij}^{Ram} E_j^{inc}(\boldsymbol{r}_a, \omega_{inc}) M_j^{loc}(\boldsymbol{r}_a, \omega_{Rad}) M_i^{loc}(\boldsymbol{r}_a, \omega_{Rad})|^2}{|\sum_{a=1}^{N_{atoms}} \sum_{i,j=1}^{3} e_i^{rad} \alpha_{a,ij}^{Ram} E_j^{inc}(\boldsymbol{r}_a, \omega_{inc})|^2} \quad (5)$$

We assume that the field enhancement depends only weakly on the vibrational frequency (due to the off-resonant illumination and the difference between incident frequency and vibrational frequencies) and thus, $M^{loc}(\boldsymbol{r}, \omega_{rad}) \approx M^{loc}(\boldsymbol{r}, \omega_{inc})$. In this case, K^{EM} depends on the vibrational mode because $\vec{\vec{\alpha}}^{Ram}$, and thus $\boldsymbol{p}^{EM}$ is specific to each mode. For homogeneous fields $M^{loc}(\boldsymbol{r}, \omega_{inc}) = M^{loc}(\omega_{inc})$, and we recover the usual proportionality between the EM enhancement factor K^{EM} and $|M^{loc}(\omega_{inc})|^4$.[65] Additionally, as we always evaluate $M^{loc}(\boldsymbol{r}, \omega_{inc})$ for an incoming planewave with electric field polarized along the z-direction, eq 4 corresponds to the emitted light polarized in this same direction.

We plot in Figure 2e−h the Raman spectra of the molecule situated in the local field induced by the gold clusters, as obtained by applying eq 4. The Raman lines of the vibrational modes ν_6, ν_{12}, ν_{15}, and ν_{28} exhibit a moderate enhancement of their Raman cross-sections as a consequence of the EM interaction (compare with the results of the isolated molecule in Figure 1a). This enhancement increases with the size of the clusters and is not the same for all of the modes, which leads to changes in the relative weight of the Raman lines. We show in Figure 2i the increase of K^{EM} with the cluster size for the selected vibrational modes. K^{EM} is larger for the vibrational mode ν_{15} than that for the other selected vibrational modes: the maximum value of K^{EM} is ≈15 for the vibrational mode ν_{15} and the dimer Au_{20}−Au_{20}, while for the other selected vibrational modes, K^{EM} never exceeds a value of ≈7. The different evolution of K^{EM} for the selected vibrational modes leads to an increase of the relative weight of the Raman line of the vibrational mode ν_{15} with cluster size in Figure 2e−h. This different evolution can be understood from the vibrational pattern of each mode and from the spatial distribution of the electric fields induced by the gold clusters. The local fields E^{loc} are larger at the tip of the tetrahedral clusters. At the same time, the vibrational mode ν_{15} corresponds to the stretching of the C−S bond (see the green rectangle in Figure 1b), which lies in regions with the largest $|E^{loc}|$.

The EM mechanism thus induces moderate changes in the relative weight of the Raman lines due to the inhomogeneity of the EM field, and it affects each vibrational mode differently, depending on the specific characteristics of the vibrational mode (atoms involved in proximity to strong local field inhomogeneities). The absolute values of the EM enhancement are relatively small in our case because we consider small clusters excited out of resonance. In larger clusters and nanoparticles, the local field enhancement will scale up with the size. The small size adopted here is convenient to compare these results with the calculation of the chemical enhancement within a full DFT scheme, as performed in the next sections.

3.3. Total SERS Enhancement. We next obtain the total SERS enhancement factor of the molecular Raman signal for the same gold−molecule complexes $[Au_n\text{-BPDT-}Au_n]^{2+}$ (n = 1, 4, 10, and 20). We select the complexes with charge +2 a. u. because in this case, the HOMO and/or the LUMO are localized in the molecule (Figure S1 of the Supporting Information), in good agreement with periodic DFT calculations showing that organosulfur compounds and gold surfaces interact through charge-transfer processes.[66,67] We show in Figure 3a−d the lowest-energy structures of these cations, obtained with DFT following the same procedure as described in the Section Theoretical Methods. In all the structures, the molecule interacts covalently with the gold cluster through the sulfur atoms.

The DFT simulation provides the induced Raman dipole, which can again be decomposed into atomic contributions, p_a^{SERS}. We then use the reciprocity theorem to account for the effect of the gold clusters on the emission from this dipole (Section S3 in the Supporting Information). The resulting Stokes differential Raman cross-section is

$$\frac{d\sigma_k^{SERS}}{d\Omega} = \frac{(\omega_{inc} - \omega_k^{SERS})^4}{16\pi^2 c_0^4 \epsilon_0^2 |E^{inc}|^2} \frac{|\sum_{a=1}^{N_{atoms}} \sum_{i=1}^{3} p_{a,i}^{SERS} M_i^{loc}(\boldsymbol{r}_a, \omega_{rad})|^2}{(1 - e^{-\hbar\omega_k^{SERS}/(k_B T)})} \quad (6)$$

In contrast to eq 2, which treats the scattering of the molecular-induced Raman dipole as if it was placed in free-space, eq 6 corresponds to the emission of the induced Raman dipole of the molecule attached to the gold clusters that enhance the local field by a factor $M_i^{loc}(\boldsymbol{r}_a, \omega_{rad})$ for the i-th component.

We show in Figure 3e−h the Raman spectra of the cations $[Au_n\text{-BPDT-}Au_n]^{2+}$ computed using eq 6 and considering $M^{loc}(\boldsymbol{r}, \omega_{rad}) \approx M^{loc}(\boldsymbol{r}, \omega_{inc})$. Here, we also select vibrational modes ν_6, ν_{12}, ν_{15}, and ν_{28}. Relative to the Raman spectrum of the free-space BPDT (Figure 1), the gold clusters generally induce energy red-shifts and changes in intensity of the Raman lines associated with these modes. These effects depend on the number of Au atoms (the magnitude of the Raman shifts can be more easily appreciated in Figure S4 of the Supporting Information). Among the selected modes, the largest Raman shifts are experienced by the vibrational modes ν_{12} and ν_{15}, which show a maximum red-shift of 58 cm^{-1} and 65 cm^{-1},

https://doi.org/10.1021/acs.jpcc.4c03491
J. Phys. Chem. C 2024, 128, 18293−18304

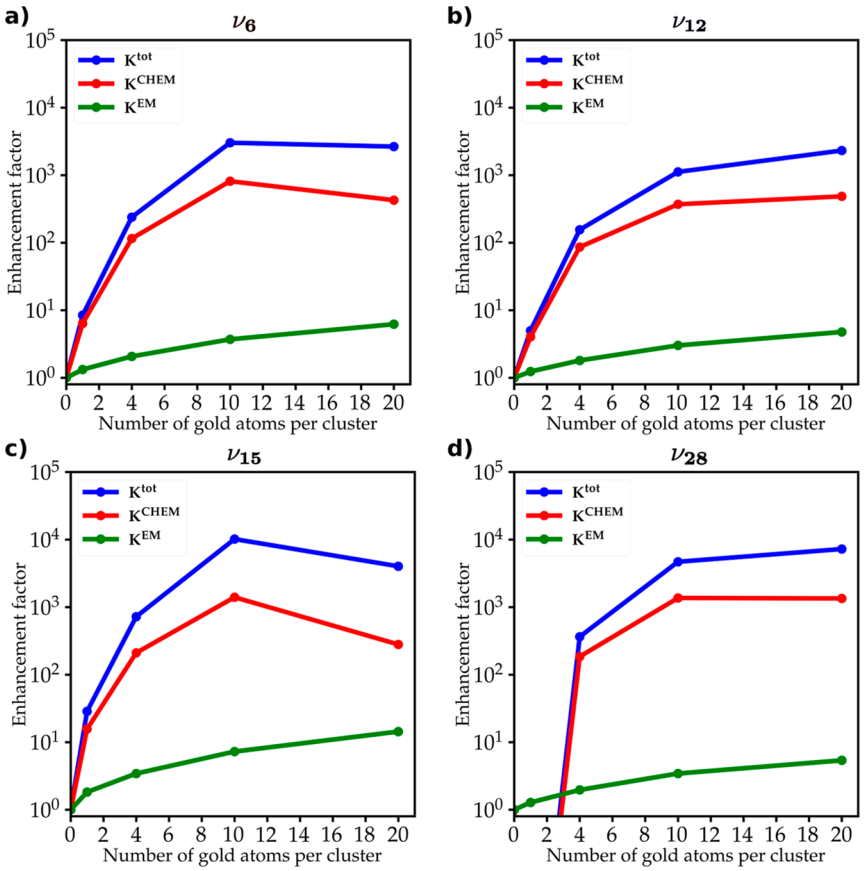

Figure 4. Enhancement factors for the selected vibrational modes as a function of the number of gold atoms per cluster: (a–d) Evolution of the total SERS enhancement factor (K^{tot}, solid blue line), the chemical enhancement factor (K^{CHEM}, solid red line), and the EM enhancement factor (K^{EM}, solid green line) for the vibration modes ν_6 (a), ν_{12} (b) ν_{15} (c), and ν_{28} (d). The values of K^{tot} and K^{EM} are the same as shown in Figure 3i and in Figure 2i, respectively, and are repeated here for easier comparison.

respectively, for the complex $[\text{Au-BPDT-Au}]^{2+}$. These two modes are characterized by combinations of C–H bending (both modes) and C–C (58 cm^{-1}) and C–S (65 cm^{-1}) stretching vibrations of BPDT. Their energies shift toward lower wavenumbers indicating a weakening of these bonds, which is consistent with the activation of charge transfer from the molecule to the clusters.

We focus next on the large enhancement of the Raman cross-section and introduce the total SERS enhancement factor (K^{tot}) for a given vibrational mode, defined as

$$K^{tot} = \frac{|\sum_{a=1}^{N_{atoms}}\sum_{i=1}^{3} p_{a,i}^{SERS} M_i^{loc}(\boldsymbol{r}_a, \omega_{inc})|^2}{|\boldsymbol{e}^{rad}\cdot\boldsymbol{p}^{Ram}|^2} = \frac{|\sum_{a=1}^{N_{atoms}}\sum_{i,j=1}^{3} \alpha_{a,ij}^{SERS} E_j^{inc}(\boldsymbol{r}_a, \omega_{inc}) M_i^{loc}(\boldsymbol{r}_a, \omega_{inc})|^2}{|\sum_{a=1}^{3}\sum_{i,j=1}^{3} e_i^{rad}\alpha_{a,ij}^{Ram} E_j^{inc}(\boldsymbol{r}_a, \omega_{inc})|^2} \quad (7)$$

with α_{ij}^{SERS} the i-th, j-th element of the atomistic Raman polarizability of the vibrational mode ν_k of $[\text{Au}_n\text{-BPDT-Au}_n]^{2+}$ (n = 1, 4, 10, and 20).

We plot in Figure 3i the evolution of K^{tot} with cluster size. K^{tot} can be as large as 10^3 for $[\text{Au}_{10}\text{-BPDT-Au}_{10}]^{2+}$ and $[\text{Au}_{20}\text{-BPDT-Au}_{20}]^{2+}$, more than 2 orders of magnitude larger than the EM enhancement K^{EM} (see Figure 2i). The values of K^{tot} generally increase with the size of the cluster, but the value and exact trend vary from mode to mode, as can be also observed from the spectral changes in the Raman spectra (Figure 3e–h) that affect the relative strength of the peaks. This effect is particularly significant for the vibrational mode ν_{28} (orange area in Figure 3e–h), which is the weakest among the selected modes in the absence of the gold clusters (orange area in Figure 1a). This vibrational mode is almost dark when the sulfur atoms of the BPDT molecule bond to a single Au atom (n = 1, $[\text{Au-BPDT-Au}]^{2+}$) due to the change in the symmetry of the molecule (the symmetry point group of the molecule transforms from C_2 in vacuum to D_{2h} in $[\text{Au-BPDT-Au}]^{2+}$). However, the corresponding total enhancement factor K^{tot} becomes large for n = 4, increases systematically with cluster size for n = 10, 20, and is the largest among the selected vibrational modes for clusters of size n = 20 atoms. This behavior is clearly reflected in the relative strength of the peaks in the Raman spectra (Figure 3e–h): the intensity of the Raman line of the mode ν_{28} becomes more and more similar to those of modes ν_{15} and ν_{12} as the size of the clusters increases from $n \geq 4$. In the next section, we study the contribution of the CHEM mechanism to the total SERS enhancement.

3.4. Chemical Enhancement. As discussed in the Introduction section, the increase of the Raman signal described by, e.g., eq 2 (or the more accurate eq 6) is often attributed exclusively to the chemical contribution, but, as shown here, it is also influenced by the EM coupling. In order to identify the enhancement due to the CHEM mechanism, we follow a simple approach and assume that the total SERS enhancement factor K^{tot} can be directly expressed as the

https://doi.org/10.1021/acs.jpcc.4c03491
J. Phys. Chem. C 2024, 128, 18293–18304

multiplication of EM K^{EM} and chemical K^{CHEM} enhancement factors. Therefore, we write K^{CHEM} as

$$K^{CHEM} = \frac{K^{tot}}{K^{EM}} = \frac{|\sum_{a=1}^{N_{atoms}} \sum_{i=1}^{3} p_{a,i}^{SERS} M_i^{loc}(\boldsymbol{r}_a, \omega_{inc})|^2}{|\sum_{a=1}^{N_{atoms}} \sum_{i=1}^{3} p_{a,i}^{EM} M_i^{loc}(\boldsymbol{r}_a, \omega_{inc})|^2} \quad (8)$$

We compare in Figure 4 the evolution of K^{CHEM} (red line), K^{tot} (blue line), and K^{EM} (green line) with the number of gold atoms per cluster for the selected vibrational modes. We find that the values of K^{CHEM} range from ∼10 for Au−Au to ∼1000 for the largest cluster (Au_{20}−Au_{20}). K^{CHEM} generally increases with cluster size, and we attribute the slight decrease from n = 10 to n = 20 for vibrational modes ν_6 (Figure 4a) and ν_{15} (Figure 4c) to a change in the orientation of the molecule relative to the gold clusters: the closest hydrogen atoms to the thiol groups (*ortho* position), which show a large contribution to the vibrational modes ν_6 and ν_{15} (see Figure 1b), are ≈0.8 Å closer to the gold clusters for the Au_{10}−Au_{10} dimer than that for the Au_{20}−Au_{20} dimer (see Figure S6 and Table S1 in the Supporting Information), thus presenting a stronger CHEM interaction. The shortening of the distance between the hydrogen atoms and the gold cluster in this case (n = 10) increases the amount of charge transferred from the clusters to the molecule and thus enhances the Raman polarizability relative to the case of n = 20 (see Section S12 of the Supporting Information for a discussion on the charge transfer in this situation).

The chemical enhancement K^{CHEM} values are significantly larger than those due to the EM interaction K^{EM}, which is a consequence of the small size of the clusters and the off-resonant illumination. Thus, K^{tot} is mostly determined by the chemical enhancement factor K^{CHEM}. This analysis thus confirms that for small clusters under non-resonant conditions, the chemical enhancement K^{CHEM} is the main contribution of the total SERS enhancement factor. However, the EM enhancement also contributes in a non-negligible way. The value of the chemical enhancement is overestimated if it is assumed to be equal to the total SERS enhancement factor obtained from the DFT calculation. Furthermore, the error introduced in this way becomes larger as progressively improved computational capabilities enable quantum mechanical calculations of the optical response of metallic clusters of increasing size. It is thus desirable to properly treat the total enhancement as standardly obtained from DFT calculations so as to isolate the pure CHEM effect.

4. SUMMARY AND CONCLUSIONS

We have shown a systematic procedure to obtain the contribution of the chemical (CHEM) mechanism to the SERS enhancement factor of the molecular Raman signal, separating it from the electromagnetic (EM) contribution. This approach makes use of DFT calculations of the molecular Raman polarizability and TDDFT calculations of the enhanced electromagnetic field induced by metallic clusters. We apply these methodologies to study the EM and CHEM contributions of four canonical molecular vibrational modes of the molecule biphenyl-4,4′-dithiol (BPDT) in a chemical environment comprising sets of two identical tetrahedral gold clusters of increasing number of gold atoms, $[Au_n\text{-BPDT-}Au_n]^{2+}$ (n = 1, 4, 10, and 20).

We first calculate the EM contribution of K^{EM} to the total SERS enhancement factor for the molecule sandwiched between the gold clusters. This calculation uses DFT to compute the Raman polarizability of the molecule under vacuum and TDDFT to compute the local EM field induced by the gold clusters (in the absence of the molecule). The value of the Raman polarizability does not affect the EM enhancement for spatially homogeneous fields, but it needs to be considered when EM fields are strongly inhomogeneous, as in our case. To take into account the local field inhomogeneity, we compute the molecular Raman polarizability as a sum of atomic contributions and obtain the local induced Raman dipole by weighting each atomic contribution by the value of the local field at the corresponding atomic position. A similar approach is followed to model the emission, where we include the enhancement of the emission from each local induced Raman dipole by using reciprocity. The use of TDDFT calculations to obtain the EM fields avoids the error that could be introduced by treating such small clusters classically and allows for a fair comparison of each effect due to the consistency of the calculations. Our results reveal that the molecular Raman signal of small $[Au_n\text{-BPDT-}Au_n]^{2+}$ cluster−molecule complexes is moderately enhanced by the EM mechanism.

We then calculate the total SERS enhancement factor K^{tot} from the Raman polarizability of the molecule attached to the gold clusters $[Au_n\text{-BPDT-}Au_n]^{2+}$, as obtained within DFT, and from the inhomogeneous local EM fields induced by the gold clusters, as calculated within TDDFT. The latter is again necessary to include the enhancement of the emission by the clusters, an effect often neglected in the literature. We find that the molecular Raman signal can be enhanced by a factor as large as 10^3 despite the moderate contribution of the EM mechanism.

Once each of the factors, K^{EM} and K^{tot} are obtained, one can proceed to the core development of this work, i.e., extracting the enhancement factor K^{CHEM} that accounts for the change in the molecular Raman signal due exclusively to the chemical interaction between the molecule and the gold clusters. To that end, we assume that the total SERS enhancement factor is given by the product of the contributions of the EM and CHEM mechanisms; therefore, we compute K^{CHEM}, as the ratio of K^{tot} and K^{EM}. Our results confirm that K^{CHEM} is the main contribution to the total SERS enhancement factor for the small clusters considered in this work. However, we emphasize that the main goal of our work is to elaborate an accurate theoretical protocol to accurately extract the chemical contribution from the total enhancement usually reported from quantum chemistry calculations. Once the CHEM enhancement factor is accurately known, it can be properly combined with full EM simulations that mimic a particular experimental situation, as is commonly carried out in the literature. To enable this improved determination of the chemical SERS enhancement factor, our proposed methodology combines DFT calculations of the molecule and TDDFT simulations of the optical response of the metallic nanostructure, including the spatial inhomogeneity of the field and enhancement by the gold clusters of the Raman emission. In standard practical situations in SERS, larger metallic nanostructures than the clusters considered here are commonly used, where the EM enhancement typically dominates, and DFT calculations of the Raman signal are not tractable. Nevertheless, the larger EM enhancements found in those situations could be classically calculated, and the result should be combined with the exact contribution from the CHEM enhancement, as extracted here.

https://doi.org/10.1021/acs.jpcc.4c03491
J. Phys. Chem. C 2024, 128, 18293−18304

Thus, this work advances toward more precise studies in advanced SERS configurations, such as in plasmonic nano- and pico-cavities.

■ ASSOCIATED CONTENT

Data Availability Statement

The data that support the findings of this study can be found at https://digital.csic.es/handle/10261/368320.

Supporting Information

The Supporting Information is available free of charge at https://pubs.acs.org/doi/10.1021/acs.jpcc.4c03491.

Frontier molecular orbitals of $[Au_n\text{-BPDT-}Au_n]^{2+}$ (n = 4, 10, 20); computation of the induced Raman dipole for inhomogeneous EM fields; derivation of the Stokes differential Raman cross-section $\frac{d\sigma_k^{SERS}}{d\Omega}$; effect of the emission process on the SERS spectra of $[Au_n\text{-BPDT-}Au_n]^{2+}$ (n = 1, 4, 10, 20); effect of the vibrations of the gold clusters on the SERS spectra of $[Au_n\text{-BPDT-}Au_n]^{2+}$ (n = 1, 4, 10, 20); effect of the gold clusters on the molecular Raman shifts of $[Au_n\text{-BPDT-}Au_n]^{2+}$ (n = 1, 4, 10, 20); details on the optimization of the molecular structure of $[Au_n\text{-BPDT-}Au_n]^{2+}$ (n = 4, 10, and 20); structural parameters of $[Au_n\text{-BPDT-}Au_n]^{2+}$ (n = 1, 4, 10, 20); influence of the DFT functional on the Raman cross-section; enhancement factors for the vibrational mode ν_{42}; effect of the relaxation of the gold clusters on the chemical structure of $[Au_n\text{-BPDT-}Au_n]^{2+}$ (n = 1, 4, and 10); analysis of the charge and polarizabilities for $[Au_n\text{-BPDT-}Au_n]^{2+}$; and Cartesian coordinates of the optimized structures (PDF)

■ AUTHOR INFORMATION

Corresponding Authors

Roberto A. Boto − *Donostia International Physics Center DIPC, Donostia-San Sebastián 20018, Spain;* orcid.org/0000-0002-8012-1499; Email: robalboto@dipc.org

Rubén Esteban − *Centro de Física de Materiales CFM-MPC (CSIC-UPV/EHU), Donostia-San Sebastián 20018, Spain; Donostia International Physics Center DIPC, Donostia-San Sebastián 20018, Spain;* orcid.org/0000-0002-9175-2878; Email: ruben.esteban@ehu.eus

Javier Aizpurua − *Donostia International Physics Center DIPC, Donostia-San Sebastián 20018, Spain; Ikerbasque, Basque Foundation for Science, Bilbao 48009, Spain; Department of Electricity and Electronics, University of the Basque Country, Leioa 48940, Spain;* orcid.org/0000-0002-1444-7589; Email: aizpurua@ehu.eus

Author

Bruno Candelas − *Centro de Física de Materiales CFM-MPC (CSIC-UPV/EHU), Donostia-San Sebastián 20018, Spain; Donostia International Physics Center DIPC, Donostia-San Sebastián 20018, Spain;* orcid.org/0000-0001-8777-4022

Complete contact information is available at: https://pubs.acs.org/10.1021/acs.jpcc.4c03491

Notes

The authors declare no competing financial interest.

■ ACKNOWLEDGMENTS

We are grateful for financial support from grant PID2022-139579NB-I00 funded by MICIU/AEI/10.13039/501100011033/and by ERDF/EU, from FET-Open project no. 829067 (THOR), and from grant no. IT 1526-22 from the Basque Government for consolidated groups of the Basque University and project Elkartek u4smart. B.C. acknowledges support through the PhD Student program of Materials Physics Center and Donostia International Physics Center.

■ REFERENCES

(1) Albrecht, M. G.; Creighton, J. A. Anomalously intense Raman spectra of pyridine at a silver electrode. *J. Am. Chem. Soc.* **1977**, *99*, 5215−5217.

(2) Jeanmaire, D. L.; Van Duyne, R. P. Surface Raman spectroelectrochemistry: Part I. Heterocyclic, aromatic, and aliphatic amines adsorbed on the anodized silver electrode. *J. Electroanal. Chem. Interfacial Electrochem.* **1977**, *84*, 1−20.

(3) Fleischmann, M.; Hendra, P. J.; McQuillan, A. J. Raman spectra of pyridine adsorbed at a silver electrode. *Chem. Phys. Lett.* **1974**, *26*, 163−166.

(4) Ma, K.; Yuen, J. M.; Shah, N. C.; Walsh, J. T., Jr; Glucksberg, M. R.; Van Duyne, R. P. In vivo, transcutaneous glucose sensing using surface-enhanced spatially offset Raman spectroscopy: multiple rats, improved hypoglycemic accuracy, low incident power, and continuous monitoring for greater than 17 days. *Anal. Chem.* **2011**, *83*, 9146−9152.

(5) Yuen, J. M.; Shah, N. C.; Walsh, J. T., Jr; Glucksberg, M. R.; Van Duyne, R. P. Transcutaneous glucose sensing by surface-enhanced spatially offset Raman spectroscopy in a rat model. *Anal. Chem.* **2010**, *82*, 8382−8385.

(6) Leong, S. X.; Leong, Y. X.; Tan, E. X.; Sim, H. Y. F.; Koh, C. S. L.; Lee, Y. H.; Chong, C.; Ng, L. S.; Chen, J. R. T.; Pang, D. W. C.; et al. Noninvasive and point-of-care surface-enhanced Raman scattering (SERS)-based breathalyzer for mass screening of coronavirus Disease 2019 (COVID-19) under 5 min. *ACS Nano* **2022**, *16*, 2629−2639.

(7) Paxton, W. F.; Kleinman, S. L.; Basuray, A. N.; Stoddart, J. F.; Van Duyne, R. P. Surface-enhanced Raman spectroelectrochemistry of TTF-modified self-assembled monolayers. *J. Phys. Chem. Lett.* **2011**, *2*, 1145−1149.

(8) Mandrile, L.; Cagnasso, I.; Berta, L.; Giovannozzi, A. M.; Petrozziello, M.; Pellegrino, F.; Asproudi, A.; Durbiano, F.; Rossi, A. M. Direct quantification of sulfur dioxide in wine by Surface Enhanced Raman Spectroscopy. *Food Chem.* **2020**, *326*, 127009.

(9) Mandrile, L.; Vona, M.; Giovannozzi, A. M.; Salafranca, J.; Martra, G.; Rossi, A. M. Migration study of organotin compounds from food packaging by surface-enhanced Raman scattering. *Talanta* **2020**, *220*, 121408.

(10) Ji, W.; Zhao, B.; Ozaki, Y. Semiconductor materials in analytical applications of surface-enhanced Raman scattering. *J. Raman Spectrosc.* **2016**, *47*, 51−58.

(11) Tan, X.; Melkersson, J.; Wu, S.; Wang, L.; Zhang, J. Noble-Metal-Free Materials for Surface-Enhanced Raman Spectroscopy Detection. *ChemPhysChem* **2016**, *17*, 2630−2639.

(12) Sharma, B.; Frontiera, R. R.; Henry, A.-I.; Ringe, E.; Van Duyne, R. P. SERS: Materials, applications, and the future. *Mater. Today* **2012**, *15*, 16−25.

(13) Moskovits, M. Surface-enhanced spectroscopy. *Rev. Mod. Phys.* **1985**, *57*, 783−826.

(14) Weitz, D.; Garoff, S.; Gersten, J.; Nitzan, A. The enhancement of Raman scattering, resonance Raman scattering, and fluorescence from molecules adsorbed on a rough silver surface. *J. Chem. Phys.* **1983**, *78*, 5324−5338.

(15) Gersten, J.; Nitzan, A. Spectroscopic properties of molecules interacting with small dielectric particles. *J. Chem. Phys.* **1981**, *75*, 1139−1152.

(16) Gersten, J. I. The effect of surface roughness on surface enhanced Raman scattering. *J. Chem. Phys.* **1980**, *72*, 5779−5780.
(17) McCall, S.; Platzman, P.; Wolff, P. Surface enhanced Raman scattering. *Phys. Lett. A* **1980**, *77*, 381−383.
(18) McCall, S.; Platzman, P. Raman scattering from chemisorbed molecules at surfaces. *Phys. Rev. B* **1980**, *22*, 1660−1662.
(19) Zeman, E. J.; Schatz, G. C. An accurate electromagnetic theory study of surface enhancement factors for silver, gold, copper, lithium, sodium, aluminum, gallium, indium, zinc, and cadmium. *J. Phys. Chem.* **1987**, *91*, 634−643.
(20) Xu, H.; Aizpurua, J.; Käll, M.; Apell, P. Electromagnetic contributions to single-molecule sensitivity in surface-enhanced Raman scattering. *Phys. Rev. E* **2000**, *62*, 4318−4324.
(21) Guillot, N.; de la Chapelle, M. L. The electromagnetic effect in surface enhanced Raman scattering: Enhancement optimization using precisely controlled nanostructures. *J. Quant. Spectrosc. Radiat. Transfer* **2012**, *113*, 2321−2333.
(22) Yamamoto, Y. S.; Ozaki, Y.; Itoh, T. Recent progress and frontiers in the electromagnetic mechanism of surface-enhanced Raman scattering. *J. Photochem. Photobiol., C* **2014**, *21*, 81−104.
(23) Alonso-González, P.; Albella, P.; Schnell, M.; Chen, J.; Huth, F.; García-Etxarri, A.; Casanova, F.; Golmar, F.; Arzubiaga, L.; Hueso, L.; et al. Resolving the electromagnetic mechanism of surface-enhanced light scattering at single hot spots. *Nat. Commun.* **2012**, *3*, 1−7.
(24) Xu, H.; Bjerneld, E. J.; Käll, M.; Börjesson, L. Spectroscopy of single hemoglobin molecules by surface enhanced Raman scattering. *Phys. Rev. Lett.* **1999**, *83*, 4357−4360.
(25) Le Ru, E. C.; Blackie, E.; Meyer, M.; Etchegoin, P. G. Surface enhanced Raman scattering enhancement factors: a comprehensive study. *J. Phys. Chem. C* **2007**, *111*, 13794−13803.
(26) Burstein, E.; Chen, Y.; Chen, C.; Lundquist, S.; Tosatti, E. Giant" Raman scattering by adsorbed molecules on metal surfaces. *Solid State Commun.* **1979**, *29*, 567−570.
(27) Billmann, J.; Otto, A. Electronic surface state contribution to surface enhanced Raman scattering. *Solid State Commun.* **1982**, *44*, 105−107.
(28) Lombardi, J. R.; Birke, R. L.; Lu, T.; Xu, J. Charge-transfer theory of surface enhanced Raman spectroscopy: Herzberg−Teller contributions. *J. Chem. Phys.* **1986**, *84*, 4174−4180.
(29) Adrian, F. J. Charge transfer effects in surface-enhanced Raman scatteringa. *J. Chem. Phys.* **1982**, *77*, 5302−5314.
(30) Otto, A. Surface enhanced Raman scattering (SERS), what do we know? *Appl. Surf. Sci.* **1980**, *6*, 309−355.
(31) Otto, A.; Mrozek, I.; Grabhorn, H.; Akemann, W. Surface-enhanced Raman scattering. *J. Phys.: Condens. Matter* **1992**, *4*, 1143−1212.
(32) Zhao, L. L.; Jensen, L.; Schatz, G. C. Surface-enhanced Raman scattering of pyrazine at the junction between two Ag20 nanoclusters. *Nano Lett.* **2006**, *6*, 1229−1234.
(33) Morton, S. M.; Jensen, L. Understanding the molecule- surface chemical coupling in SERS. *J. Am. Chem. Soc.* **2009**, *131*, 4090−4098.
(34) Moore, J. E.; Morton, S. M.; Jensen, L. Importance of correctly describing charge-transfer excitations for understanding the chemical effect in SERS. *J. Phys. Chem. Lett.* **2012**, *3*, 2470−2475.
(35) Zhao, J.; Pinchuk, A. O.; McMahon, J. M.; Li, S.; Ausman, L. K.; Atkinson, A. L.; Schatz, G. C. Methods for describing the electromagnetic properties of silver and gold nanoparticles. *Acc. Chem. Res.* **2008**, *41*, 1710−1720.
(36) Fiederling, K.; Abasifard, M.; Richter, M.; Deckert, V.; Kupfer, S.; Grafe, S. A full quantum mechanical approach assessing the chemical and electromagnetic effect in TERS. *ACS Nano* **2023**, *17*, 13137−13146.
(37) Trivedi, D. J.; Barrow, B.; Schatz, G. C. Understanding the chemical contribution to the enhancement mechanism in SERS: Connection with Hammett parameters. *J. Chem. Phys.* **2020**, *153*, 124706.
(38) Chen, R.; Jensen, L. Interpreting chemical enhancements of surface-enhanced Raman scattering. *Chem. Phys. Rev.* **2023**, *4*, 021305.
(39) Gieseking, R. L.; Ratner, M. A.; Schatz, G. C. Theoretical modeling of voltage effects and the chemical mechanism in surface-enhanced Raman scattering. *Faraday Discuss.* **2017**, *205*, 149−171.
(40) Benz, F.; Schmidt, M. K.; Dreismann, A.; Chikkaraddy, R.; Zhang, Y.; Demetriadou, A.; Carnegie, C.; Ohadi, H.; de Nijs, B.; Esteban, R.; et al. Single-molecule optomechanics in "picocavities. *Science* **2016**, *354*, 726−729.
(41) Zhang, Y.; Dong, Z.-C.; Aizpurua, J. Theoretical treatment of single-molecule scanning Raman picoscopy in strongly inhomogeneous near fields. *J. Raman Spectrosc.* **2021**, *52*, 296−309.
(42) Frisch, M. J.; et al. *Gaussian 16*, Revision B.01; Gaussian Inc: Wallingford CT, 2016.
(43) Beck, A. D. Density-functional thermochemistry. III. The role of exact exchange. *J. Chem. Phys.* **1993**, *98*, 5648−5656.
(44) Perdew, J. P. Density-functional approximation for the correlation energy of the inhomogeneous electron gas. *Phys. Rev. B* **1986**, *33*, 8822−8824.
(45) Neugebauer, J.; Hess, B. A. Fundamental vibrational frequencies of small polyatomic molecules from density-functional calculations and vibrational perturbation theory. *J. Chem. Phys.* **2003**, *118*, 7215−7225.
(46) Hay, P. J.; Wadt, W. R. Ab initio effective core potentials for molecular calculations. Potentials for K to Au including the outermost core orbitals. *J. Chem. Phys.* **1985**, *82*, 299−310.
(47) Petersson, G.; Al-Laham, M. A. A complete basis set model chemistry. II. Open-shell systems and the total energies of the first-row atoms. *J. Chem. Phys.* **1991**, *94*, 6081−6090.
(48) Grimme, S.; Antony, J.; Ehrlich, S.; Krieg, H. A consistent and accurate ab initio parametrization of density functional dispersion correction (DFT-D) for the 94 elements H-Pu. *J. Chem. Phys.* **2010**, *132*, 154104.
(49) Grimme, S.; Ehrlich, S.; Goerigk, L. Effect of the damping function in dispersion corrected density functional theory. *J. Comput. Chem.* **2011**, *32*, 1456−1465.
(50) Soler, J. M.; Artacho, E.; Gale, J. D.; García, A.; Junquera, J.; Ordejón, P.; Sánchez-Portal, D. The SIESTA method for ab initio order-N materials simulation. *J. Phys.: Condens. Matter* **2002**, *14*, 2745−2779.
(51) Perdew, J. P.; Burke, K.; Ernzerhof, M. Generalized gradient approximation made simple. *Phys. Rev. Lett.* **1996**, *77*, 3865−3868.
(52) Perdew, J. P.; Burke, K.; Ernzerhof, M. Generalized Gradient Approximation Made Simple [Phys. Rev. Lett. 77, 3865 (1996)]. *Phys. Rev. Lett.* **1997**, *78*, 1396.
(53) Urbieta, M.; Barbry, M.; Zhang, Y.; Koval, P.; Sánchez-Portal, D.; Zabala, N.; Aizpurua, J. Atomic-scale lightning rod effect in plasmonic picocavities: A classical view to a quantum effect. *ACS Nano* **2018**, *12*, 585−595.
(54) Koval, P.; Barbry, M.; Sánchez-Portal, D. PySCF-NAO: An efficient and flexible implementation of linear response time-dependent density functional theory with numerical atomic orbitals. *Comput. Phys. Commun.* **2019**, *236*, 188−204.
(55) Yanai, T.; Tew, D. P.; Handy, N. C. A new hybrid exchange−correlation functional using the Coulomb-attenuating method (CAM-B3LYP). *Chem. Phys. Lett.* **2004**, *393*, 51−57.
(56) Le Ru, E. C.; Etchegoin, P. G. *Principles of Surface-Enhanced*; Elsevier: 2008.
(57) Mulliken, R. S. Report on notation for the spectra of polyatomic molecules. *J. Chem. Phys.* **1955**, *23*, 1997−2011.
(58) Neugebauer, J.; Reiher, M.; Kind, C.; Hess, B. A. Quantum chemical calculation of vibrational spectra of large molecules—Raman and IR spectra for buckminsterfullerene. *J. Comput. Chem.* **2002**, *23*, 895−910.
(59) Jensen, L.; Zhao, L. L.; Schatz, G. C. Size-Dependence of the Enhanced Raman Scattering of Pyridine Adsorbed on Ag$_n$ (n = 2−8, 20) Clusters. *J. Phys. Chem. C* **2007**, *111*, 4756−4764.
(60) Mandado, M.; Ramos-Berdullas, N. Confinement on the optical response in h-BNCs: Towards highly efficient SERS-active 2D substrates. *Spectrochim. Acta, Part A* **2022**, *266*, 120451.

https://doi.org/10.1021/acs.jpcc.4c03491
J. Phys. Chem. C 2024, 128, 18293−18304

(61) López-Carballeira, D.; Ramos-Berdullas, N.; Pérez-Juste, I.; Mandado, M. Can single graphene nanodisks be used as Raman enhancement platforms? *RSC Adv.* **2016**, *6*, 71397−71403.
(62) Ramos-Berdullas, N.; Otero, N.; Mandado, M. Graphene Molecules as Platforms for SERS Detection: A Future Perspective. *Handbook of Graphene, Volume 6: Biosensors and Advanced Sensors*; 2019, *431*, 429−464..
(63) Aikens, C. M.; Madison, L. R.; Schatz, G. C. The effect of field gradient on SERS. *Nat. Photonics* **2013**, *7*, 508−510.
(64) Chulhai, D. V.; Jensen, L. Determining molecular orientation with surface-enhanced Raman scattering using inhomogenous electric fields. *J. Phys. Chem. C* **2013**, *117*, 19622−19631.
(65) Le Ru, E.; Etchegoin, P. Rigorous justification of the $|E|^4$ enhancement factor in Surface Enhanced Raman Spectroscopy. *Chem. Phys. Lett.* **2006**, *423*, 63−66.
(66) Peiretti, L. F.; Quaino, P.; Tielens, F. Competition between two high-density assemblies of poly (phenyl) thiols on Au (111). *J. Phys. Chem. C* **2016**, *120*, 25462−25472.
(67) Barzaga, R.; Hernández, M. P.; Aguilar-Galindo, F.; Díaz-Tendero, S. Revealing the Interplay Between Covalent and Non-Covalent Interactions Driving the Adsorption of Monosubstituted Thiourea Derivatives on the Au (111) Surface. *J. Phys. Chem. C* **2020**, *124*, 9924−9939.

https://doi.org/10.1021/acs.jpcc.4c03491
J. Phys. Chem. C 2024, 128, 18293−18304